JACS
JOURNAL OF THE AMERICAN CHEMICAL SOCIETY
pubs.acs.org/JACS
Article

Probing the Electronic Structure and Bond Dissociation of SO_3 and SO_3^- Using High-Resolution Cryogenic Photoelectron Imaging

Dao-Fu Yuan,[§] Tarek Trabelsi,[§] Yue-Rou Zhang, Joseph S. Francisco,* and Lai-Sheng Wang*

Cite This: J. Am. Chem. Soc. 2022, 144, 13740−13747
Read Online
ACCESS | Metrics & More | Article Recommendations | Supporting Information

ABSTRACT: The SO_3 molecule and its radical anion SO_3^- are important chemical species atmospherically. However, their thermodynamic properties and electronic structures are not well known experimentally. Using cryogenically cooled anions, we have obtained high-resolution photoelectron images of SO_3^- and determined accurately the electron affinity (EA) of SO_3 and the bond dissociation energy of $SO_3^- \rightarrow SO_2 + O^-$ for the first time. Because of the large geometry changes from the C_{3v} SO_3^- to the D_{3h} SO_3, there is a negligible Franck−Condon factor (FCF) for the 0−0 detachment transition, that defines the EA of SO_3. By fitting the high-resolution photoelectron spectra with computed FCFs using structures from high-level ab initio calculations, we have determined the EA of SO_3 to be 2.126(6) eV. By monitoring the appearance of the O^- signal in the photoelectron images at different photon energies, we are able to measure directly the bond dissociation energy of $SO_3^-(X^2A_1) \rightarrow SO_2(X^1A_1) + O^-(^2P)$ to be 4.259 ± 0.006 eV, which also allow us to derive the dissociation energy for the spin-forbidden $SO_3(X^1A_1') \rightarrow SO_2(X^1A_1) + O(^3P)$ to be 3.594(6) eV. The excited states of SO_3^- are calculated using high-level ab initio calculations, which are valuable in aiding the interpretation of autodetachment processes observed at various photon energies. The current study provides valuable information about the fundamental molecular properties of SO_3, as well as the radical anion SO_3^-, which is known in redox reactions involving SO_3^{2-} and may also play a role in the chemistry of SO_2 in the atmosphere.

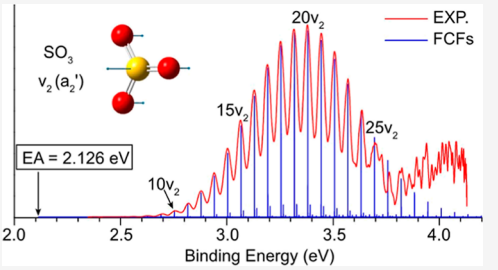

INTRODUCTION

It is well known that sulfur-containing compounds play important roles in atmospheric chemistry and are major precursors of the acid rain and atmospheric aerosols.[1−4] As one of the key intermediates in the gas-phase oxidation of SO_2 to form sulfuric acid,[1,5] the sulfur trioxide (SO_3) molecule has attracted significant interest and has been extensively studied experimentally[6−10] and theoretically.[11−14] Sulfur is one of the most abundant elements in the universe, and various sulfur compounds, including SO_2, have been detected extraterrestrially and in the interstellar medium.[15,16] Irradiation of SO_2 ice has resulted in the formation of SO_3,[17] suggesting that SO_3 or its anion may also exist in the interstellar medium. SO_3 is a planar molecule with D_{3h} symmetry in its ground electronic state (X^1A_1'). Vibrational frequencies of SO_3 have been accurately measured in the gas phase by infrared (IR) and Raman spectroscopies.[18−21] The photochemistry and photodissociation of SO_3 have been investigated in the ultraviolet (UV) and vacuum ultraviolet (VUV) regions.[22−24]

The radical anion of SO_3 (SO_3^-) is also important in various chemical processes, from the aqueous redox of SO_3^{2-} to the environmental and atmospheric chemistry of SO_2.[25,26] However, in contrast to SO_3, the spectroscopy and photochemistry of SO_3^- have been much less studied.[27−33] UV absorption spectra in aqueous solution[27] and IR studies with matrix isolation[28] were reported. In the gas phase, the electron affinity (EA) of SO_3 was estimated from collisional ionization methods (≥1.7 ± 0.15 eV)[29] and electron transfer experiments (1.9 ± 0.1 eV).[34] Photoelectron spectroscopy (PES) of SO_3^- at 355 and 266 nm was first reported in 2000 by Dobrin et al.[32] A broad band due to a long progression in the ν_2 umbrella mode was observed as a result of the large geometry change from the C_{3v} SO_3^- to the D_{3h} SO_3. Dobrin et al. was only able to report the vertical detachment energy (VDE) of SO_3^- (3.41 ± 0.01 eV) and the observation of photodissociation of $SO_3^- \rightarrow SO_2 + O^-$ at 266 nm. Recently, a photoelectron imaging study of SO_3^- was carried out by Anstöter and Verlet (AV),[33] who reported the photoelectron angular distributions (PADs) and energy-dependent anisotropy parameters.

PES of negative ions is an important technique to probe the electronic structure, EA, and vibrational information of the corresponding neutral species.[35−37] However, it was not possible to determine the EA of SO_3 in the two previous PES studies[32,33] because of the negligible Franck−Condon factor (FCF) for the 0−0 detachment transition that defines the EA. In addition, the limited experimental resolution and

Received: May 2, 2022
Published: July 20, 2022

https://doi.org/10.1021/jacs.2c04698
J. Am. Chem. Soc. 2022, 144, 13740−13747

hot bands caused significant spectral broadening, making it difficult to do FCF fitting in the previous PES studies. Consequently, no EA for SO_3 was reported in the two previous PES studies, and the 1.9 ± 0.1 eV EA value quoted from ref 30 in the previous PES studies was, in fact, from an unpublished result.[34] Thus, the EA of SO_3 still remains poorly known.

One of the major motivations of the current study is to determine the EA of SO_3 using our high-resolution photoelectron (PE) imaging apparatus equipped with a cryogenically controlled ion trap.[38] In addition to the good resolution of our imaging system, vibrationally cold SO_3^- anions are essential to resolve a clean ν_2 bending vibrational progression, which would facilitate FCF fitting for the determination of the EA. In addition, we are also interested in examining the photon energy dependence of the $SO_3^- \rightarrow SO_2 + O^-$ dissociation channel observed previously by Dobrin et al.,[32] in order to estimate the bond dissociation energy in conjunction with high-level theoretical calculations.

We have obtained high-resolution PE images and spectra of cryogenically cooled SO_3^- at a wide range of photon energies and calculated the excited states of SO_3^- using high-level ab initio methods. The well-resolved PE spectra allowed us to determine accurately the EA of SO_3 to be 2.126 ± 0.006 eV from FCF simulations. By monitoring the appearance of the O^- signal, we are able to measure directly the bond dissociation energy of $SO_3^-(X^2A_1) \rightarrow SO_2(X^1A_1) + O^-(^2P)$ to be 4.259 ± 0.006 eV, which in turn allowed us to obtain the dissociation energy of the spin-forbidden dissociation channel $SO_3(X^1A_1') \rightarrow SO_2(X^1A_1) + O(^3P)$ to be 3.594 ± 0.006 eV. PES at different photon energies showed autodetachment processes due to optical transitions to the excited states of the SO_3^- anion. All experimental observations are corroborated by high-level ab initio calculations of the potential energy curves (PECs) of SO_3^- and its electronically excited states.

Experimental Methods. The experiment was carried out using our high-resolution electrospray ionization-PES (ESI-PES) apparatus equipped with a cryogenically cooled Paul trap.[38,39] The SO_3^- anions were produced by electrospray of a 1 mM solution of sodium bisulfite (Sigma-Aldrich) in a mixed solvent of CH_3OH/H_2O (~4/1 in volume) at pH ~ 3. Anions generated in the ESI source were guided into a cryogenically cooled 3D Paul trap operated at 4.6 K.[38] After being accumulated for 0.1 s and thermally cooled via collisions with a 1 mTorr He/H_2 (4/1 in volume) background gas,[39] the anions were pulsed out at a 10 Hz repetition rate into the extraction zone of a time-of-flight mass spectrometer. A small amount of SO_3^- anions were formed due to the decomposition of bisulfite during ESI and were selected by a mass gate and photodetached in the interaction zone of a velocity-map imaging lens[40] by a tunable dye laser (fundamental or frequency-doubled output) or the fourth harmonic (266 nm) of an Nd:YAG laser. The polarization direction of the detachment laser was parallel to the imaging plane. Photoelectrons were projected onto a pair of 75 mm diameter microchannel plates coupled to a phosphor screen and captured by a charge-coupled-device camera. The PE images were inverse-Abel transformed and reconstructed using the pBasex[41] and BASEX[42] programs. The PE spectra were calibrated with the known spectra of Au^- at different photon energies. The kinetic energy (KE) resolution was 3.8 cm^{-1} for electrons with 55 cm^{-1} KE and about 1.5% (ΔKE/KE) for KE above 1 eV in the current experiment.[38]

The resolution of the PE images depends on the extraction voltage on the imaging lens.[40] Lower extraction voltages give better resolution, but higher voltages are needed for the detection of fast electrons. In the current experiment, the extraction voltage used was 600 V for photon energies below 3 eV and 1000 V for photon energies above 3 eV. A higher voltage (1400 V) was required to detect PE signals from the $O^-(^2P)$ fragment in the dissociation threshold measurement.

Theoretical Methods. The electronic structures and energetics of SO_3^- and SO_3 were computed using highly correlated ab initio multireference and single-reference methods and large basis sets.[43,44] For the investigation of the electronic structure of the SO_3 ground state, we used coupled cluster theory with perturbative treatment of triple excitations CCSD(T).[45,46] Because of the diffuse nature of the negative ions, the atoms were described using a diffuse basis set of aug-cc-pV(X+d)Z (X = T and Q) quality.[47,48] The potential energies of the ground and the low-lying electronic states of neutral SO_3 and the SO_3^- anion along the S−O stretching coordinates were computed with the highly accurate multireference multiconfigurational methodology, that is, complete-active-space self-consistent field CASSCF[49,50] followed by the multireference configuration interaction with Davidson correction MRCI + Q.[51,52] In these calculations, the atoms were described by aug-cc-pVTZ and extra tight d functions for the sulfur atom. These calculations were carried out in the C_s point group and with the full valence active space. In the CASSCF procedure, two states were averaged per state symmetry. For the excited-state calculations, the dissociation limit was calculated at the CCSD(T)/aug-cc-pV(Q+d)Z level due to the non-size consistency of the MRCI + Q method. Finally, the calculated PECs were calibrated with the dissociation limit, and the EA was calculated at the CCSD(T) level. The reader may refer to our previous work[43,44] for more information about the construction of the PECs for the negative ion. For the optimized equilibrium geometries of the lowest states, all configurations in the CI expansion of the CASSCF wave function having a weight larger than 0.001 were considered.

RESULTS

Photoelectron Images and Spectra of SO_3^-. The PE images and spectra of SO_3^- at five photon energies between 3.1608 and 4.1294 eV are shown in Figure 1. A broad vibrational progression due to the ν_2 umbrella mode was observed between 2.5 and 3.8 eV. The PE images displayed beautiful p-wave angular distributions, consistent with the σ-type SOMO (a_1) of SO_3^- (Figure S1). The broad FC envelope agrees with the previous PES studies[32,33] but much better resolved due to both the higher spectral resolution of the current PE imaging apparatus and the cryogenically cooled SO_3^- anions. The positions of all the resolved vibrational peaks (labeled from A to T in Figure 1e) are summarized in Table S1. The average separation of the vibrational peaks for the ν_2 mode is measured to be 505 ± 5 cm^{-1}, compared to a value of 548 ± 80 cm^{-1} reported previously by Dobrin et al.[32] and 517 ± 10 cm^{-1} by AV.[33] The VDE defined by peak N was measured to be 3.379 ± 0.003 eV, compared to the previously reported value of 3.41 ± 0.01 eV[32] and 3.4 ± 0.1 eV.[33] In the spectra, as shown in Figure 1, the 0−0 transition was clearly not observed. The lowest discernible peak A was at 2.563 eV, which was much higher than the expected EA of SO_3.

https://doi.org/10.1021/jacs.2c04698
J. Am. Chem. Soc. 2022, 144, 13740−13747

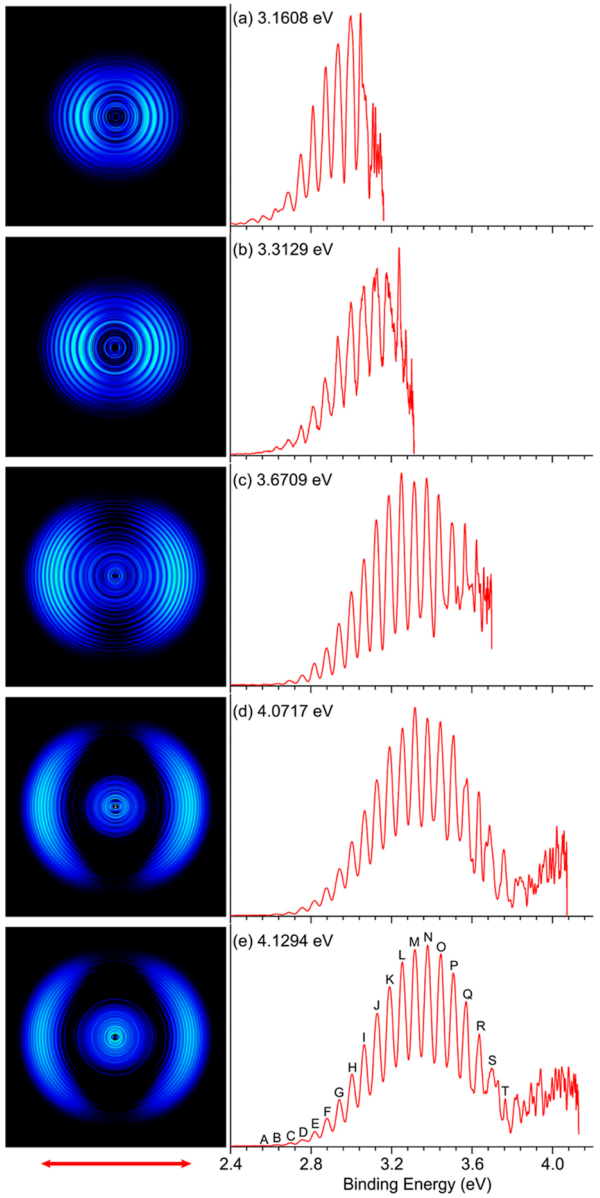

Figure 1. PE images and spectra of SO_3^- at (a) 3.1608, (b) 3.3129, (c) 3.6709, (d) 4.0717, and (e) 4.1294 eV. The red arrow below the image represents the polarization direction of the detachment laser.

In Figure 1d,e, a weak feature is observed on the high binding energy side above ~3.8 eV. The PE images corresponding to these signals (the central feature in the images) displayed near-isotropic angular distributions. A similar broad feature was also observed by AV for spectra with photon energies above ~4 eV,[33] and they interpreted the continuous signals as thermionic emission, that is, photoabsorption to an anion excited state followed by conversion to the ground electronic state of the anion accompanied by electron emission from the highly vibrationally excited anion.

PE Images and Spectra of SO_3^- at Low Photon Energies. The PE spectra in Figure 1 showed very weak signals below ~2.5 eV, which was still much higher than the expected EA of SO_3.[29,34] Attempting to observe the 0−0 detachment transition and measure the EA of SO_3, we took two spectra at lower photon energies (2.6678 and 2.7264 eV), as shown in Figure 2. We expected to see the ν_2 vibrational progression extended to lower binding energies, approaching

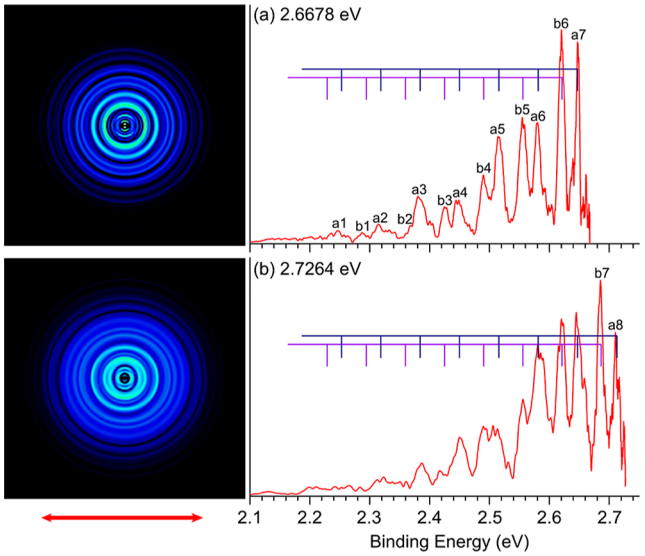

Figure 2. PE images and spectra of SO_3^- at (a) 2.6678 eV and (b) 2.7264 eV. Note the different angular distributions and vibrational progressions in comparison to those in Figure 1.

the 0−0 transition. Surprisingly, the spectra in Figure 2 display completely different vibrational patterns. Two equally spaced vibrational progressions are observed and labeled as peaks a1−a8 and b1−b7, respectively. The peak positions of the two progressions are given in Table S2. The energy separation for each progression is determined to be 530 ± 15 cm^{-1}, and the separation between the two progressions is 215 ± 15 cm^{-1}. Furthermore, the PE images display isotropic angular distributions, instead of the p-wave feature observed in Figure 1 at higher photon energies. Very weak signals could be detected at around 2.2 eV, but a clear 0−0 transition was still elusive.

PE Image and Spectrum of SO_3^- at 266 nm. We also measured the PE image of SO_3^- at 266 nm (4.661 eV), as shown in Figure 3, in order to compare with that reported by

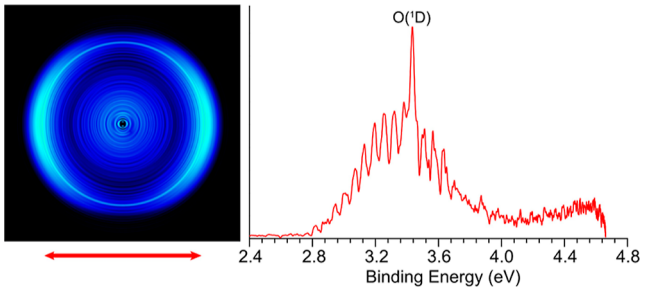

Figure 3. PE image and spectrum of SO_3^- at 266 nm (4.661 eV). The peak at 3.43 eV, labeled as $O(^1D)$, came from the detachment of $O^-(^2P)$ to $O(^1D)$ due to photodissociation of SO_3^- + 266 nm → $SO_2(X^1A_1)$ + $O^-(^2P)$. Note the detachment channel to the $O(^3P)$ ground state expected at 1.46 eV was not shown and not observed due to the low extraction voltage on the imaging lens.

Dobrin et al.[32] The broad ν_2 vibrational progression was similar to those observed in Figure 1d,e. However, an extra intense peak at 3.43 eV, labeled as $O(^1D)$, was also observed, overlapping with the p-wave vibrational progression. The angular distribution of the extra peak was clearly different from that of the ν_2 progression. This extra peak came from

https://doi.org/10.1021/jacs.2c04698
J. Am. Chem. Soc. 2022, 144, 13740−13747

detachment from $O^-(^2P)$ to $O(^1D)$, as a result of photodissociation of $SO_3^- \rightarrow SO_2(X^1A_1) + O^-(^2P)$ at 266 nm, exactly as reported by Dobrin et al.[32] The spectrum in Figure 3 was taken with an extraction voltage of 1000 V to optimize the spectral resolution. However, it was too low for the detachment channel to the $O(^3P)$ ground state (~3.2 eV KE or 1.46 eV in binding energy). The weak continuous signals on the high binding energy side are similar to those observed in Figure 1d,e, and they are also likely due to thermionic emission.

Theoretical PECs. The PECs of the ground and low-lying excited states along the S−O stretching coordinate of neutral SO_3 and the SO_3^- anion were calculated at the MRCI + Q/aug-cc-pV(T+d)Z level, as shown in Figure 4. The ground

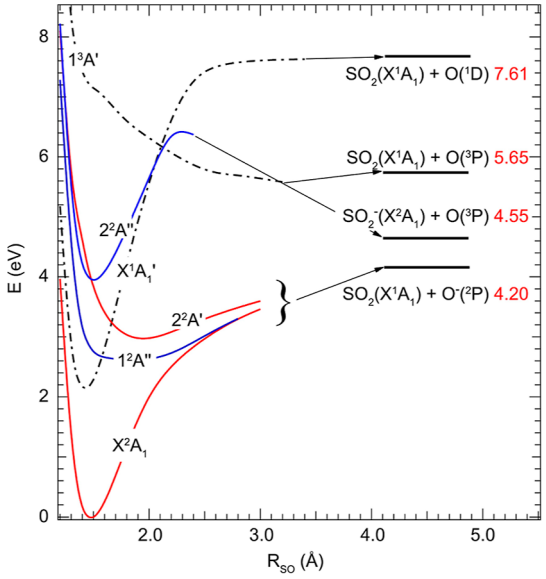

Figure 4. MRCI + Q/aug-cc-pV(T+d)Z PEC of the low-lying electronic states of SO_3 (black dashed lines) and SO_3^- (red and blue lines) along the S−O stretching coordinate. The remaining coordinates were kept fixed at their optimized equilibrium geometries at the CCSD(T)/aug-cc-pV(T+d)Z level.

state of SO_3^- is fully below the ground state of the neutral because there is only a slight S−O bond length change from the anion to the neutral, R_{SO} = 1.4748 Å for SO_3^- versus 1.4231 Å for SO_3 at the CCSD(T) level (Table S3). The ground state PEC of SO_3^- correlates to the first dissociation limit of $SO_2(X^1A_1) + O^-(^2P)$, which is below the first dissociation limit of the neutral products $SO_2(X^1A_1) + O(^3P)$. The first $1^2A''$ and second $2^2A'$ excited states of SO_3^- each show a minimum in a relatively flat potential, which both correlate to the same dissociation limit as the ground state. They are crossed by the neutral PEC at R_{SO} = 1.499 Å and R_{SO} = 1.589 Å, respectively. The equilibrium geometries of the $1^2A''$ and $2^2A'$ excited states are given in Table S4. The computed vibrational frequencies for the ground states of SO_3 and SO_3^- are given in Tables S5 and S6, respectively.

For the first and the second excited states, we are interested in the part of the PECs below the neutral potential. The region above the potential of the neutral, that is, for R_{SO} < 1.499 Å for the $1^2A''$ state and R_{SO} < 1.589 Å for the $2^2A'$ state, should lead directly to autodetachment. Absorption of a photon to these two states may also lead to dissociation to the $SO_2(X^1A_1)$ + $O^-(^2P)$ products.

Analyses of the vertical excitation energy and oscillator strength show that the $1^2A'' \leftarrow X^2A_1$ transition occurs at 2.75 eV (450.9 nm), which is characterized by zero oscillator strength and weak transition dipole moment of around 0.07 Debye. At the MRCI + Q/aug-cc-pV(T+d)Z level, the global minimum of the $1^2A''$ state in the multi-dimensional potential energy surface is located at 1.61 eV above the ground state. The $2^2A' \leftarrow X^2A_1$ transition is calculated to occur at 3.84 eV (322.9 nm) and is characterized by a relatively large transition dipole moment of 0.99 Debye and oscillator strength of 0.01. The third excited state $2^2A''$ is located totally above the ground state of the neutral, correlating to the $SO_2^-(X^2A_1) + O(^3P)$ dissociation limit.

DISCUSSION

Determination of the EA of SO_3. The broad vibrational progression between 2.5 and 3.8 eV in Figure 1 corresponds to the vertical detachment from the ground electronic state of the C_{3v} $SO_3^-(X^2A_1)$ to highly vibrationally excited levels of the D_{3h} $SO_3(X^1A_1')$. Both the symmetric stretching ν_1 (a_1') mode and the umbrella mode ν_2 (a_2') (Figure S2) are FC active. Electron addition to the planar SO_3 leads to the substantial geometry changes. At the CCSD(T) level, the dihedral angle is changed to 133.8 from 180°, and the S−O bond distance is increased from 1.4231 to 1.4748 Å. Thus, the SO_3 neutral is far from equilibrium upon vertical electron detachment from the SO_3^- anion. The vibrational progression (Figure 1) should be due to the ν_2 umbrella mode with small contributions from the ν_1 mode. The VDE defined by peak N in Figure 1 was measured accurately to be 3.379 ± 0.003 eV. Using the well-defined peaks of D to S in Figure 1, we obtained an average spacing of 505 ± 5 cm^{-1}, in good agreement with the ν_2 frequency (497.6 cm^{-1}) determined by gas-phase IR spectroscopy.[21]

In order to determine the EA of SO_3, we calculated the FCFs for the detachment transition using our experimental ν_2 spacing and the theoretical geometries at the CCSD(T) level (Table S3). The calculated FCFs are overlaid on the experimental spectrum (at 4.1294 eV), as shown in Figure 5,

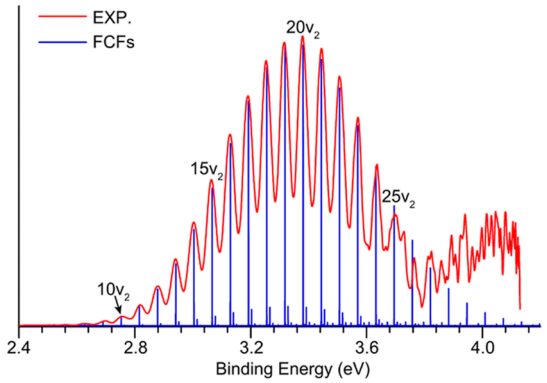

Figure 5. Comparison between the computed FCFs (blue sticks) and the experimental spectrum of SO_3^- at 4.1294 eV (red).

by aligning the peak with the highest FCF to peak N. The FCFs are dominated by the broad ν_2 vibrational progression with small contributions from the ν_1 mode. Due to the huge geometry change, the VDE corresponds to v = 20 of the ν_2 mode. The first observable peak A in Figure 1 corresponds to v = 7 of the ν_2 mode. We found that the FCF pattern is sensitive to the ν_2 frequency used. If we used the SO_3 fundamental ν_2

https://doi.org/10.1021/jacs.2c04698
J. Am. Chem. Soc. 2022, 144, 13740−13747

frequency of 497.6 cm^{-1}, the FCF pattern fits poorly to the experimental spectrum. The 505 cm^{-1} frequency gives the best fit, as shown in Figure 5. Thus, the ν_2 mode is fairly harmonic likely with a small negative anharmonicity.

The FCF fit gives rise to a 0−0 transition at 2.126 eV, which defines the EA of SO_3. Considering the small anharmonicity, we can determine with confidence the EA of SO_3 to be 2.126 ± 0.006 eV, which agrees well with our calculated value of 2.16 eV at the CCSD(T)/aug-cc-pV(Q+d)Z level (Table S7). The measured VDE of 3.379 eV is also in excellent agreement with our calculated VDE of 3.36 eV at the same level of theory.

PE Angular Distributions. The differential detachment cross section for randomly oriented molecules with linearly polarized light can be expressed as[53]

$$I(\theta) = \sigma_T/4\pi[1 + \beta P_2(\cos\theta)] \quad (1)$$

where σ_T is the total detachment cross section, β ($-1 < \beta < 2$) is the anisotropy parameter that describes the PAD, $P_2(\cos\theta)$ is the second-order Legendre polynomial, and θ is the angle between the ejected photoelectron and the polarization direction of the detachment laser. $\beta = 0$ results in an isotropic s outgoing wave, whereas $\beta = -1$ gives rise to an (s + d) wave with the maximum intensity in the direction perpendicular to the laser polarization. $\beta = 2$ represents a p-wave detachment with the maximum intensity along the laser polarization.

The β parameters of the vibrational peaks in the spectra at 4.1294 eV are derived from the high-resolution image shown in Figure 1e, as presented in Figure 6 (blue circle) as a function

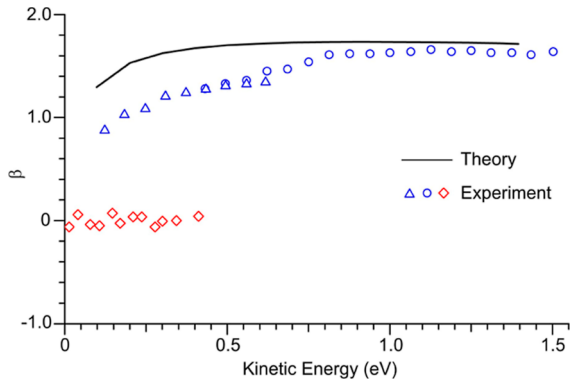

Figure 6. Measured β parameters compared with the calculated values (solid line) as a function of electron KE.[31] The measured values are determined from the spectra at 4.1294 eV (blue circle), 3.3129 eV (blue triangle), and 2.7264 eV (red diamond).

of the PE KE. The β values obtained from the spectrum at 3.3129 eV (Figure 1b) are also included to cover the KE below 0.4 eV (Figure 6, blue triangle). The experimentally measured β values are in good agreement with the calculations (solid line in Figure 6) reported by Anstöter et al.[31] The β parameter displays a weak dependence on the electron KE on the low-energy side.

For the PE spectra taken at photon energies higher than ~4.0 eV (Figures 1d,e and 3), a continuous and isotropic feature ($\beta \sim 0$) above ~3.8 eV is observed. This broad feature could not be due to an excited state of SO_3 by detaching an electron from the HOMO of SO_3^- (Figure S1) because the computed first excited state of SO_3 ($1^3A'$, as shown in Figure 4) is considerably higher in energy. Furthermore, the HOMO with a_2 symmetry is primarily an O 2p lone pair and should result in a (s + d)-wave PAD, rather than an isotropic PAD. The broad and isotropic feature suggests that it should come from a secondary process. It was attributed to thermionic emission by AV.[33] This is plausible because the photon energies are above the first two excited states of SO_3^- (Figure 4). Most likely, this feature was due to excitation to the optically allowed $2^2A'$ excited state, followed by conversion to the ground state, resulting in electron emission from highly vibrationally excited anions. Furthermore, autodetachment from the $2^2A'$ excited state of SO_3^- to the ground state of $SO_3(X^1A_1')$ could also contribute to this feature.

Autodetachment at Lower Photon Energies. The two spectra, as shown in Figure 2, at 2.6678 and 2.7264 eV displayed completely different vibrational structures as those in Figure 1. The two vibrational progressions (a1−a8 and b1−b7) both have an average separation of 530 ± 15 cm^{-1}, which agrees with the in-plane bending mode ν_4 (e′, Figure S2) of SO_3 with a frequency of 530.1 cm^{-1}.[21] Furthermore, these two spectra exhibited isotropic PADs ($\beta \sim 0$, red diamond in Figure 6), instead of the expected p-wave distribution. The isotropic signals suggested indirect detachment processes, that is, autodetachment from an excited state of SO_3^-. Our calculations show that the vertical excitation energy of the first excited electronic state of SO_3^- ($1^2A''$) is around 2.75 eV (Figure 4, Table S8), consistent with the photon energies used for the spectra in Figure 2. Our calculations revealed that the $1^2A'' \leftarrow X^2A'$ transition is optically forbidden, in agreement with the very weak signals observed. The $1^2A''$ excited state has C_1 symmetry (Table S4); thus, the ν_4 bending mode is FC-allowed during autodetachment.

It is interesting to note that the first observable peak a1 at 2.248 ± 0.009 eV is separated from the 0−0 transition (2.126 eV) by 0.122 eV (984 cm^{-1}). Considering the large uncertainty in the binding energy of the weak a1 peak, this separation almost exactly represents two quanta of the ν_4 mode, that is, the a1 peak is the $v = 2$ level of the ν_4 mode. The b1 peak at 2.289 ± 0.007 eV is separated from the 0−0 transition by 0.163 eV (1315 cm^{-1}), which is close to the known frequency of the ν_3 mode (1391.5 cm^{-1}).[21] Thus, the b1-b7 progression is likely due to a combinational series with one quantum of the ν_3 mode, that is, $\nu_3^1\nu_4^v$. These observations indirectly confirm the validity of the derived 0−0 transition from the FCF fitting discussed above.

Measurement of the $SO_3^- \rightarrow SO_2 + O^-$ Dissociation Energy. The $O(^1D)$ signal in the 266 nm spectrum of SO_3^- (Figure 3) is due to the detachment from the dissociation product $O^-(^2P)$, as first observed by Dobrin et al.[32] The dissociative state is most likely the $2^2A'$ excited state of SO_3^- via direct excitation to this state or internal conversion from the forbidden $2^2A''$ excited state (Figure 4). The observation of PE signals from the O^- fragment anion provides a promising way to directly measure the dissociation energy of $SO_3^-(X^2A') \rightarrow SO_2(X^1A_1) + O^-(^2P)$ by monitoring the O^- signals as a function of photon energy.

To search for the dissociation threshold of SO_3^- and avoid the influence of the strong direct detachment signals of the parent anion, we monitored the appearance of the $O(^3P)$ ground-state signal from detachment from the $O^-(^2P)$ fragment. Due to the high electron KE (low binding energy) of this detachment channel, we had to use a high extraction voltage on the imaging lens, resulting in slightly lower spectral resolution, as shown in Figure 7. The intensity of the $O(^3P)$ signal at 1.46 eV is very sensitive to the excitation energy. It is

https://doi.org/10.1021/jacs.2c04698
J. Am. Chem. Soc. 2022, 144, 13740−13747

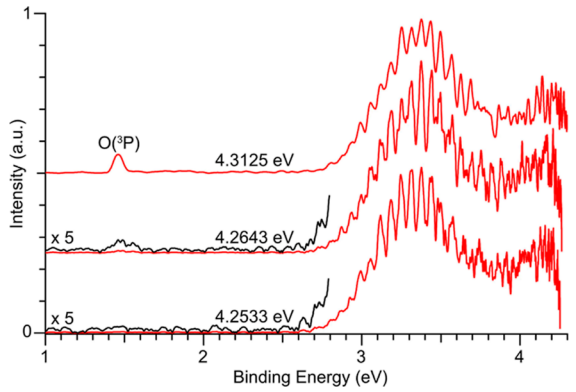

Figure 7. PE spectra of SO_3^- at 4.3125, 4.2643, and 4.2533 eV. The baselines of the spectra at 4.2643 and 4.3125 eV are shifted by 0.25 and 0.5 (arbitrary unit), respectively.

relatively strong at 4.3125 eV, becomes very weak at 4.2643 eV, and disappears at a slightly lower photon energy at 4.2533 eV. Therefore, the dissociation energy of SO_3^- is between 4.2533 and 4.2643 eV, that is 4.259 ± 0.006 eV, which agrees well with the predicted value of 4.204 eV at the CCSD(T)/aug-cc-pV(Q+d)Z level of theory.

Using the EA of SO_3 (2.126 ± 0.006 eV) and the dissociation energy of SO_3^- (4.259 ± 0.006 eV) from the current study and the known EA of the oxygen atom (1.461 eV),[54] we can evaluate the dissociation energy of $SO_3(X^1A_1')$ to the spin-forbidden products $SO_2(X^1A_1)$ + $O(^3P)$, as illustrated in Scheme 1: $EA(SO_3) + D(SO_3) = D(SO_3^-) + EA(O)$. The evaluated dissociation energy for $SO_3(X^1A_1') \rightarrow SO_2(X^1A_1) + O(^3P)$ is 3.594 ± 0.006 eV. Using the excitation energy of $O(^1D)$ (1.967 eV), we evaluated the dissociation energy of $SO_3(X^1A')$ to the spin-allowed products $SO_2(X^1A_1)$ + $O(^1D)$ to be 5.561 ± 0.006 eV. Even though the photodissociation of SO_3 has been studied,[22] the dissociation energies of SO_3 have not been directly measured. Our derived dissociation energies of 3.594 ± 0.006 eV and 5.561 ± 0.006 eV for the two dissociation channels are in agreement with the values of 3.606 eV and 5.576 eV, respectively, estimated from the thermochemical data.[55] This agreement also confirms our determined EA for SO_3 and the dissociation energy for SO_3^-.

Scheme 1. Schematic of the Thermodynamic Cycle for $SO_3^-(X^2A') \rightarrow SO_2(X^1A_1) + O(^3P) + e$

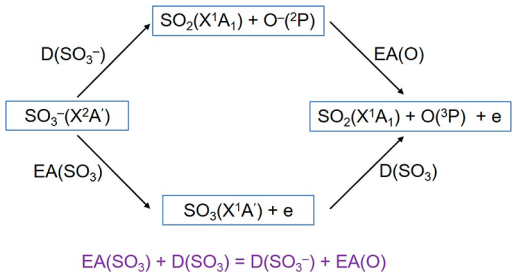

CONCLUSIONS

In conclusion, we report a combined high-resolution photoelectron imaging and theoretical study of SO_3^- using cryogenically cooled anions and high-level ab initio calculations. The well-resolved vibrational progression in the photoelectron spectra for the ν_2 umbrella mode is used to compare with Franck−Condon simulations, allowing us to determine the EA of SO_3 to be 2.126 ± 0.006 eV for the first time. By monitoring the appearance of the O^- photoelectron signals, we are able to directly measure the dissociation energy for $SO_3^-(X^2A') \rightarrow SO_2(X^1A_1) + O^-(^2P)$. The obtained EA of SO_3 and the dissociation energy of SO_3^- also allowed us to determine the dissociation energy of $SO_3(X^1A_1') \rightarrow SO_2(X^1A_1) + O(^3P)$. The excited-state manifold computed for SO_3^- allowed us to understand the various autodetachment processes. The thermodynamics and spectroscopic information obtained in the current work will be valuable to understand the photophysics and chemistry of SO_3 and its radical anion both terrestrially and extraterrestrially.

ASSOCIATED CONTENT

Supporting Information

The Supporting Information is available free of charge at https://pubs.acs.org/doi/10.1021/jacs.2c04698.

Additional experimental and theoretical results (PDF)

AUTHOR INFORMATION

Corresponding Authors

Joseph S. Francisco − *Department of Earth and Environmental Sciences and Department of Chemistry, University of Pennsylvania, Philadelphia, Pennsylvania 19104, United States;* orcid.org/0000-0002-5461-1486; Email: frjoseph@sas.upenn.edu

Lai-Sheng Wang − *Department of Chemistry, Brown University, Providence, Rhode Island 02912, United States;* orcid.org/0000-0003-1816-5738; Email: Lai-Sheng_Wang@brown.edu

Authors

Dao-Fu Yuan − *Department of Chemistry, Brown University, Providence, Rhode Island 02912, United States;* orcid.org/0000-0001-8461-6889

Tarek Trabelsi − *Department of Earth and Environmental Sciences and Department of Chemistry, University of Pennsylvania, Philadelphia, Pennsylvania 19104, United States;* orcid.org/0000-0001-6258-7191

Yue-Rou Zhang − *Department of Chemistry, Brown University, Providence, Rhode Island 02912, United States*

Complete contact information is available at: https://pubs.acs.org/10.1021/jacs.2c04698

Author Contributions

[§]D.-F.Y. and T.T. contributed equally to this work.

Notes

The authors declare no competing financial interest.

ACKNOWLEDGMENTS

This work was supported by the U.S. Department of Energy, Office of Basic Energy Sciences, Chemical Sciences, Geosciences, and Biosciences Division under grant DE-SC0018679 (to L.-S.W.).

REFERENCES

(1) Wayne, R. P. *Chemistry of Atmospheres: An Introduction to the Chemistry of the Atmospheres of Earth, the Planets, and Their Satellites (3rd Edition)*; Oxford University Press: New York, 2000; pp 7−11.

(2) Henning, S.; Ziese, M.; Kiselev, A.; Saathoff, H.; Möhler, O.; Mentel, T. F.; Buchholz, A.; Spindler, C.; Michaud, V.; Monier, M.;

Sellegri, K.; Stratmann, F. Hygroscopic Growth and Droplet Activation of Soot Particles: Uncoated, Succinic or Sulfuric Acid Coated. *Atmos. Chem. Phys.* **2012**, *12*, 4525−4537.
(3) Khalizov, A. F.; Zhang, R.; Zhang, D.; Xue, H.; Pagels, J.; McMurry, P. H. Formation of Highly Hygroscopic Soot Aerosols upon Internal Mixing with Sulfuric Acid Vapor. *J. Geophys. Res.* **2009**, *114*, D05208.
(4) Ehn, M.; Petäjä, T.; Aufmhoff, H.; Aalto, P.; Hämeri, K.; Arnold, F.; Laaksonen, A.; Kulmala, M. Hygroscopic Properties of Ultrafine Aerosol Particles in the Boreal Forest: Diurnal Variation, Solubility and the Influence of Sulfuric Acid. *Atmos. Chem. Phys.* **2007**, *7*, 211−222.
(5) Carmona-García, J.; Trabelsi, T.; Francés-Monerris, A.; Cuevas, C. A.; Saiz-Lopez, A.; Roca-Sanjuán, D.; Francisco, J. S. Photochemistry of $HOSO_2$ and SO_3 and Implications for the Production of Sulfuric Acid. *J. Am. Chem. Soc.* **2021**, *143*, 18794−18802.
(6) Kolb, C. E.; Jayne, J. T.; Worsnop, D. R.; Molina, M. J.; Meads, R. F.; Viggiano, A. A. Gas Phase Reaction of Sulfur Trioxide with Water Vapor. *J. Am. Chem. Soc.* **1994**, *116*, 10314−10315.
(7) Jayne, J. T.; Pöschl, U.; Chen, Y.; Dai, D.; Molina, L. T.; Worsnop, D. R.; Kolb, C. E.; Molina, M. J. Pressure and Temperature Dependence of the Gas-Phase Reaction of SO_3 with H_2O and the Heterogeneous Reaction of SO_3 with H_2O/H_2SO_4 Surfaces. *J. Phys. Chem. A* **1997**, *101*, 10000−10011.
(8) Lovejoy, E. R.; Hanson, D. R.; Huey, L. G. Kinetics and Products of the Gas-Phase Reaction of SO_3 with Water. *J. Phys. Chem.* **1996**, *100*, 19911−19916.
(9) Pommerening, C. A.; Bachrach, S. M.; Sunderlin, L. S. Addition of Protonated Water to SO_3. *J. Phys. Chem. A* **1999**, *103*, 1214−1220.
(10) Robert Lloyd, D.; Roberts, P. J.; Hillier, I. H.; Shenton, I. C. On the Photoelectron Spectrum of Sulphur Trioxide. *Mol. Phys.* **1976**, *31*, 1549−1556.
(11) Meijer, E. J.; Sprik, M. A Density Functional Study of the Addition of Water to SO_3 in the Gas Phase and in Aqueous Solution. *J. Phys. Chem. A* **1998**, *102*, 2893−2898.
(12) Morokuma, K.; Muguruma, C. Ab Initio Molecular Orbital Study of the Mechanism of the Gas Phase Reaction $SO_3 + H_2O$: Importance of the Second Water Molecule. *J. Am. Chem. Soc.* **1994**, *116*, 10316−10317.
(13) Hofmann, M.; Schleyer, P. v. R. Acid Rain: Ab Initio Investigation of the $H_2O{\cdot}SO_3$ Complex and Its Conversion to H_2SO_4. *J. Am. Chem. Soc.* **1994**, *116*, 4947−4952.
(14) Hazra, M. K.; Sinha, A. Formic Acid Catalyzed Hydrolysis of SO_3 in the Gas Phase: A Barrierless Mechanism for Sulfuric Acid Production of Potential Atmospheric Importance. *J. Am. Chem. Soc.* **2011**, *133*, 17444−17453.
(15) Keane, J. V.; Boonman, A. M. S.; Tielens, A. G. G. M.; van Dishoeck, E. F. Gas-Phase SO_2 in Absorption Towards Massive Protostars. *Astron. Astrophys.* **2001**, *376*, L5−L8.
(16) Martín, S.; Mauersberger, R.; Martín-Pintado, J.; García-Burillo, S.; Henkel, C. First Detections of Extragalactic SO2, NS, and NO. *Astron. Astrophys.* **2003**, *411*, L465−L468.
(17) Mifsud, D.; Kaňuchová, Z.; Herczku, P.; Ioppolo, S.; Juhász, Z.; Kovács, S. T. S.; Mason, N. J.; McCullough, R. W.; Sulik, B. Sulfur Ice Astrochemistry: A Review of Laboratory Studies. *Space Sci. Rev.* **2021**, *217*, 14.
(18) Ortigoso, J.; Escribano, R.; Maki, A. G. The v_2 and v_4 IR Bands of SO_3. *J. Mol. Spectrosc.* **1989**, *138*, 602−613.
(19) Kaldor, A.; Maki, A. G.; Dorney, A. J.; Mills, I. M. The Assignment of v_2 and v_4 of SO_3. *J. Mol. Spectrosc.* **1973**, *45*, 247−252.
(20) Henfrey, N. F.; Thrush, B. A. The v_3 Band of SO_3 at High Resolution. *Chem. Phys. Lett.* **1983**, *102*, 135−138.
(21) Chrysostom, E. T. H.; Vulpanovici, N.; Masiello, T.; Barber, J.; Nibler, J. W.; Weber, A.; Maki, A.; Blake, T. A. Coherent Raman and Infrared Studies of Sulfur Trioxide. *J. Mol. Spectrosc.* **2001**, *210*, 233−239.
(22) Thelen, M.-A.; Huber, J. R. Photodissociation of SO_3 at 193 nm Investigated by Photofragment Translational Spectroscopy. *Chem. Phys. Lett.* **1995**, *236*, 558−563.
(23) Suto, M.; Ye, C.; Ram, R. S.; Lee, L. C. Sulfur Dioxide Fluorescence from Vacuum Ultraviolet Dissociative Excitation of Sulfur Trioxide. *J. Phys. Chem.* **1987**, *91*, 3262−3265.
(24) Burkholder, J. B.; McKeen, S. UV Absorption Cross Sections for SO_3. *Geophys. Res. Lett.* **1997**, *24*, 3201−3204.
(25) Wilmarth, W. K.; Stanbury, D. M.; Byrd, J. E.; Po, H. N.; Chua, C.-P. Electron-Transfer Reactions Involving Simple Free Radicals. *Coord. Chem. Rev.* **1983**, *51*, 155−179.
(26) Arnold, S. T.; Morris, R. A.; Viggiano, A. A.; Jayne, J. T. Ion Chemistry Relevant for Chemical Ionization Detection of SO_3. *J. Geophys. Res.* **1995**, *100*, 14141−14146.
(27) Hayon, E.; Treinin, A.; Wilf, J. Electronic Spectra, Photochemistry, and Autoxidation Mechanism of the Sulfite-Bisulfite-Pyrosulfite Systems. SO_2^-, SO_3^-, SO_4^-, and SO_5^- Radicals. *J. Am. Chem. Soc.* **1972**, *94*, 47−57.
(28) Stanbury, D. M.; Holme, T. A.; Kafafi, Z. H.; Margrave, J. L. Ab Initio Calculations and Matrix FTIR Studies of the Sulfur Trioxide Radical Anion. *Chem. Phys. Lett.* **1986**, *129*, 181−185.
(29) Rothe, E. W.; Tang, S. Y.; Reck, G. P. Measurement of Electron Affinities of O_3, SO_2, and SO_3 by Collisional Ionization. *J. Chem. Phys* **1975**, *62*, 3829−3831.
(30) Miller, T. M.; Viggiano, A. A.; Arnold, S. T.; Jayne, J. T. Thermal electron attachment to SO3. *J. Chem. Phys.* **1995**, *102*, 6021−6023.
(31) Ding, C. F.; Wang, X. B.; Wang, L. S. Photodetachment Photoelectron Spectroscopy of Doubly Charged Anions: $S_2O_8^{2-}$. *J. Chem. Phys.* **1999**, *110*, 3635−3638.
(32) Dobrin, S.; Boo, B. H.; Alconcel, L. S.; Continetti, R. E. Photoelectron Spectroscopy of SO_3^- at 355 and 266 nm. *J. Phys. Chem. A* **2000**, *104*, 10695−10700.
(33) Anstöter, C. S.; Verlet, J. R. R. Photoelectron Imaging of the SO_3 Anion: Vibrational Resolution in Photoelectron Angular Distributions. *Mol. Phys.* **2021**, *119*, No. e1821921.
(34) Gleason, J. F. Chemical Ionization Detection of Sulfurous Acid and the Kinetics of the Reaction Sulfurous Acid + Oxygen, Ph.D Dissertation, University of Colorado, Boulder, CO, 1987.
(35) Lineberger, W. C. Once Upon Anion: A Tale of Photodetachment. *Annu. Rev. Phys. Chem.* **2013**, *64*, 21−36.
(36) Wang, L. S. Photoelectron Spectroscopy of Size-Selected Boron Clusters: From Planar Structures to Borophenes and Borospherenes. *Int. Rev. Phys. Chem.* **2016**, *35*, 69−142.
(37) Weichman, M. L.; Neumark, D. M. Slow Photoelectron Velocity-Map Imaging of Cryogenically Cooled Anions. *Annu. Rev. Phys. Chem.* **2018**, *69*, 101−124.
(38) Wang, L. S. Perspective: Electrospray photoelectron spectroscopy: From multiply-charged anions to ultracold anions. *J. Chem. Phys.* **2015**, *143*, 040901.
(39) Wang, X. B.; Wang, L. S. Development of a Low-Temperature Photoelectron Spectroscopy Instrument Using an Electrospray Ion Source and a Cryogenically Controlled Ion Trap. *Rev. Sci. Instrum.* **2008**, *79*, 073108.
(40) León, I.; Yang, Z.; Liu, H. T.; Wang, L. S. The Design and Construction of a High-Resolution Velocity-Map Imaging Apparatus for Photoelectron Spectroscopy Studies of Size-Selected Clusters. *Rev. Sci. Instrum.* **2014**, *85*, 083106.
(41) Garcia, G. A.; Nahon, L.; Powis, I. Two-Dimensional Charged Particle Image Inversion Using a Polar Basis Function Expansion. *Rev. Sci. Instrum.* **2004**, *75*, 4989−4996.
(42) Dribinski, V.; Ossadtchi, A.; Mandelshtam, V. A.; Reisler, H. Reconstruction of Abel-Transformable Images: the Gaussian Basis-Set Expansion Abel Transform Method. *Rev. Sci. Instrum.* **2002**, *73*, 2634−2642.
(43) Trabelsi, T.; Yazidi, O.; Francisco, J. S.; Linguerri, R.; Hochlaf, M. Electronic Structure of NSO^- and SNO^- Anions: Stability, Electron Affinity, and Spectroscopic Properties. *J. Chem. Phys.* **2015**, *143*, 164301.
(44) Trabelsi, T.; Ajili, Y.; Ben Yaghlane, S.; Jaidane, N.-E.; Mogren Al-Mogren, M.; Francisco, J. S.; Hochlaf, M. Characterization and Reactivity of the Weakly Bound Complexes of the $[H, N, S]^-$ Anionic

https://doi.org/10.1021/jacs.2c04698
J. Am. Chem. Soc. 2022, 144, 13740−13747

System with Astrophysical and Biological Implications. *J. Chem. Phys.* **2015**, *143*, 034303.
(45) Knowles, P. J.; Hampel, C.; Werner, H. Coupled Cluster Theory for High Spin, Open Shell Reference Wave Functions. *J. Chem. Phys.* **1993**, *99*, 5219−5227.
(46) Knowles, P. J.; Hampel, C.; Werner, H.-J. Erratum: "Coupled Cluster Theory for High Spin, Open Shell Reference Wave Functions" [J. Chem. Phys. 99, 5219 (1993)]. *J. Chem. Phys.* **2000**, *112*, 3106−5227.
(47) Woon, D. E.; Dunning, T. H. Gaussian Basis Sets for Use in Correlated Molecular Calculations. III. The Atoms Aluminum through Argon. *J. Chem. Phys.* **1993**, *98*, 1358−1371.
(48) Dunning, T. H.; Peterson, K. A.; Wilson, A. K. Gaussian Basis Sets for Use in Correlated Molecular Calculations. X. The Atoms Aluminum through Argon Revisited. *J. Chem. Phys.* **2001**, *114*, 9244−9253.
(49) Werner, H.; Knowles, P. J. A Second Order Multiconfiguration SCF Procedure with Optimum Convergence. *J. Chem. Phys.* **1985**, *82*, 5053−5063.
(50) Knowles, P. J.; Werner, H.-J. An Efficient Second-Order MC SCF Method for Long Configuration Expansions. *Chem. Phys. Lett.* **1985**, *115*, 259−267.
(51) Werner, H.; Knowles, P. J. An Efficient Internally Contracted Multiconfiguration Reference Configuration Interaction Method. *J. Chem. Phys.* **1988**, *89*, 5803−5814.
(52) Knowles, P. J.; Werner, H.-J. An Efficient Method for the Evaluation of Coupling Coefficients in Configuration Interaction Calculations. *Chem. Phys. Lett.* **1988**, *145*, 514−522.
(53) Cooper, J.; Zare, R. N. Angular Distribution of Photoelectrons. *J. Chem. Phys.* **1968**, *48*, 942−943.
(54) Neumark, D. M.; Lykke, K. R.; Andersen, T.; Lineberger, W. C. Laser Photodetachment Measurement of the Electron Affinity of Atomic Oxygen. *Phys. Rev. A* **1985**, *32*, 1890−1892.
(55) JANAF Thermochemical Tables. *J. Phys. Chem. Ref. Data* **1985**, *14*, 177.

https://doi.org/10.1021/jacs.2c04698
J. Am. Chem. Soc. 2022, 144, 13740−13747